

Adaptive feedback control in deep brain stimulation: a simulation study

Sabato Santaniello, Giovanni Fiengo and Luigi Glielmo

Dipartimento di Ingegneria, Università del Sannio, Benevento, Italy
ssantani@unisannio.it, gifiengo@unisannio.it, glielmo@unisannio.it

Abstract: Deep brain stimulation (DBS) is an effective electric therapy to treat movement disorders associated with chronic neural diseases like essential tremor, dystonia and Parkinson's disease. In spite of a long clinical experience, the cellular effects of the DBS are still partially unknown because of the lack of information about the target sites. Recent studies, however, have proposed the local field potentials (LFPs) in the targets as a useful tool to study the behavior before and after stimulation [Priori et al., 2006].

Our work investigates the relationship between DBS settings and LFPs in a detailed simulator of the electric activity in the Vim (one of the preferred surgical targets) under tremor conditions. A least-square approach is adopted to identify a functional, input-output ARX model structure for the Vim and evaluate the effects of the stimulation on its electric patterns. Based on it, an adaptive minimum variance control scheme is then proposed to restore the spectral features of the Vim's LFPs to reference values, i.e., as in subjects not affected by movement disorders. Results indicate good performances in tracking the reference spectral features through selective changes in the low (2-7 Hz), α (7-13 Hz) and β (13-35 Hz) ranges.

Keywords: Identification; control of physiological variables; disease control; neurosystems; chronic therapy.

1. INTRODUCTION

Deep brain stimulation (DBS) is an electric therapy introduced about 15 years ago and currently used in Neurology to treat the motor symptoms associated with chronic degenerative diseases, like essential tremor (ET), dystonia, and Parkinson's disease (PD). It consists of a regular high frequency stimulation of specific subcortical sites involved in the movement-related neural patterns of the extrapyramidal system [Halpern et al., 2007]. Constant-width current pulses are generated at a frequency between 130 and 185 Hz by an implanted neural stimulator and delivered through subcutaneous wires and microelectrodes to one among the subthalamic nucleus (STN), the internal part of the globus pallidus (GPi) or the nucleus ventralis intermediate of thalamus (Vim) [Anderson et al., 2005, Kumar et al., 2003]. The choice of the target depends on the type of disease to be treated, with the Vim usually preferred in the case of essential or parkinsonian tremor and the motor part of STN or GPi in case of dystonia or PD [Wichmann, and DeLong, 2006]. Associated with an appropriate pharmacological therapy, DBS greatly reduces most of the motor symptoms, limits drug-induced dyskinesia, and frequently improves patients' ability to perform activities of daily living with less encumbrance from motor fluctuations.

Though several studies have investigated the electric properties of thalamic, subthalamic, and pallidal neurons and the corresponding neural anatomical patterns, e.g., [Destexhe et al., 1998, Beurrier et al., 1999, Nambu, and Llínas, 1994, Sato et al., 2000], how DBS works is still

partly unknown. Numerical simulations involving detailed 3D models of the neurons in the Vim ([McIntyre et al., 2004a]) and the STN ([Miocinovic et al., 2006]) predict that DBS would selectively activate large diameter fibers by suppressing intrinsic firing in the somas and eliciting an efferent output at the stimulus frequency in the axons. The independence of firing in the cell bodies and axons is then suggested as a possible explanation of apparently contradictory experimental results about the effects of DBS in primates (e.g., [Dostrovsky, and Lozano, 2002, Hashimoto et al., 2003]). However, a true validation of these results at the cellular level is difficult at the moment, due to the size and location of the nuclei of interest, whose exact identification and targeting is a challenging task. Moreover, several functionally distinct neural pathways run through them and produce a complicated arborization and reciprocal electrical and chemical influences [Sato et al., 2000]. As a consequence, it is hard to numerically reproduce scenarios that exactly match settings from *in vivo* experiments, and predict to what extent topology of the cellular interactions and synapses may influence the effects of the stimulation on single cells.

These considerations may account for the methodological and technical constraints that affect all the approaches currently adopted in literature to improve DBS efficacy, safety and power consumption. In particular, state-of-the-art knowledge prevents from a thorough comprehension of the motor and neural effects induced by changes in the parameters of stimulation (e.g., frequency, amplitude and pulse-width). Studies on ET [Kuncel et al., 2006] and PD patients [Moro et al., 2002] prove a nonlinear dependency

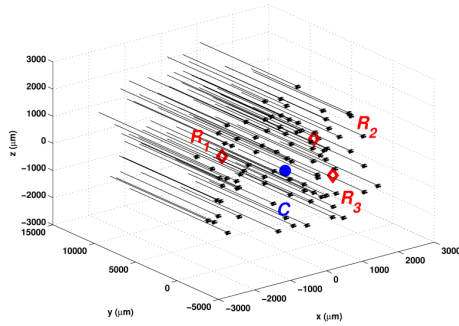


Fig. 1. 100 TC relay neurons uniformly distributed within 3 mm from a stimulating point source electrode (C , ●). 3 distinct LFPs recording electrodes are placed within 2 mm from C (R_i with $i = 1, 2, 3$, ◇).

of tremor intensity (ET case), bradykinesia and rigidity (PD case) on frequency/amplitude of stimulation, and show that safety and efficacy increase when short-width pulses are used. However, since the main causes for that are still partly unknown, no quantitative constraint can be derived for the design of the stimulus waveform.

In such a context, the goal of our work is twofold: firstly, it aims at proving that, independently of the physiologic knowledge of the cellular mechanisms in neurons, an effective phenomenological description of the tremor conditions and the DBS effects can be achieved by exploiting a marker of the actual overall state of the subject. Then, starting from such a model, it is shown that a feedback control scheme can be useful to restore healthy conditions through an automatic tuning of the DBS parameters. In details, the extracellular local electric potentials (also called “local field potentials”, LFPs [Kandel et al., 2000]), recordable at the site of stimulation by DBS-like electrodes, are used as a measure of the actual conditions in PD patients, and are related to the delivered stimulus waveform (input) through a linear autoregressive (ARX) input-output (I-O) model [Ljung, 1999]. A generalized minimum variance control law, then, compares the LFPs with a reference signal and, based on that model, modulates the input current. A self-tuning scheme [Bittanti, and Campi, 1994] is adopted to recursively update the model and controller parameters in order to improve the overall performances.

Our approach was proved in simulation on a detailed reconstruction of the neural electric activity in the human Vim around the DBS electrode under PD conditions. The Vim was chosen due to the strong cause-effect relationship between Vim’s electric activity and forearm tremor proved in PD patients [Lenz et al., 1988], and the efficacy of the DBS for tremor suppression. In fact, physiologic maps from [Hua, and Lenz, 2005] proved that the thalamocortical (TC) relay neurons in the Vim respond either to active or passive movements, while single unit analysis in [Lenz et al., 1988, Magnin et al., 2000] showed that the Vim cells fire bursts of spikes with the same frequency as the forearm tremor and phase-locked with it in PD patients. The reference signal, instead, was numerically built from experimental single-unit data recorded in the Vim of people not affected by motor disorders and whose pathologies

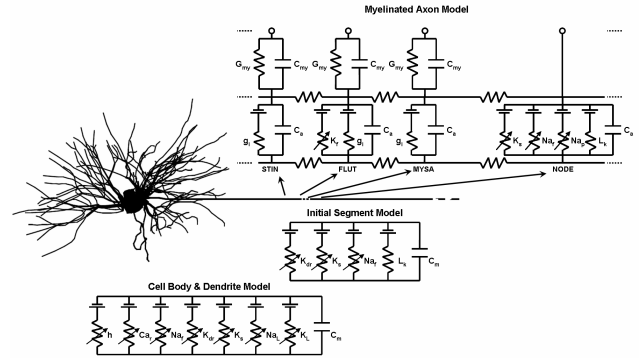


Fig. 2. Cable model of the TC relay neuron [McIntyre et al., 2004a]. MYSA=myelin attachment segment; FLUT=paranodal segment; STIN=internodal segment; NODE=node of Ranvier.

presumably do not affect the firing properties of the motor part of the Vim [Molnar et al., 2005].

2. METHODS

The study assumed that a stimulating point source electrode (C in Fig. 1) was inserted in an infinite homogeneous isotropic volume conductor (resistivity $\rho = 500 \Omega\text{-cm}$) where several TC relay neurons were randomly and uniformly placed within 3 mm from C (the distance from the stimulating electrode to each neuron was defined between C and the center element of the cell body). A multi-compartment cable model of the TC relay neuron (Fig. 2) with explicit 3D geometrical representation of the dendritic arbor, cell body, and myelinated axon and nonlinear membrane dynamics was used [McIntyre et al., 2004a]. Geometry of the compartments was obtained from the 3D reconstruction of a filled cell [Destexhe et al., 1998]. The extracellular potential (LFP) generated in the surrounding space by the superposition of the electric activity of the dendrites, paranodes, and nodes of Ranvier from each neuron was computed in different points for several stimulation settings. Stimulus profiles and induced LFPs allowed to study the overall cellular activity as a function of the applied stimulus.

In details, the effects of the point source stimuli applied in C on the neurons were computed by assigning to each compartment the potential induced at its position. Due to the 3D geometry (i.e., each compartment had a different position in the space), the responses of cells at the same absolute distance from the electrode were heterogeneous. Similarly, the LFPs induced in the extracellular volume by the concurrent activity of the neurons were simulated by representing each compartment as a point source of current, whose amplitude was set to the net transmembrane current value. At any point P , then, the LFP was:

$$\phi(P, t) = \sum_{k=1}^N \sum_{h=1}^l \frac{\rho I_{k,h}(t)}{4\pi r_{k,h}(P)}, \quad (1)$$

where $\phi(P, t)$ is the LFP evaluated in P at time t , $I_{k,h}(t)$ is the net transmembrane current in the h -th compartment of the k -th neuron at time t , $r_{k,h}(P)$ is the absolute distance of such compartment from P , N the total number of neurons, and l is the number of compartments for each neuron. No connections or interactions between the

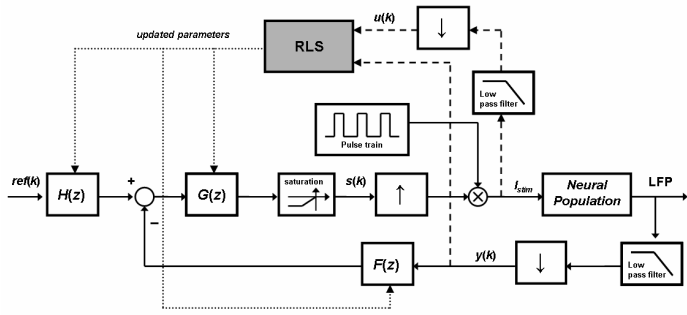


Fig. 3. Self-tuning control scheme. \downarrow = downsampling. \uparrow = upsampling. RLS = identification procedure using the RLS algorithm.

neurons were assumed. The LFPs were evaluated in 3 points uniformly chosen within 2 mm from C (R_i , $i = 1, 2, 3$ in Fig. 1) to test the dependence of the LFP spectral properties on the LFP recording location.

The simulations were performed on 3 different populations of $N = 100$ TC relay neurons for comparison purposes, and run in NEURON environment [Carnevale, and Hines, 2006]. The TC relay neuron model was integrated with CVODE (step 0.02 ms). The LFPs were computed at each time step and recorded at 25 kHz to reduce memory requirements. Analysis and signal processing were performed in MATLAB[®] (Mathworks, Natick, MA).

2.1 Simulation of PD Tremor Conditions

The intrinsic firing/bursting activity of the neurons meant to mimic the behavior of real cells recorded in the Vim of PD patients with tremor at rest [Magnin et al., 2000], and was simulated by injecting ad hoc designed intracellular pseudo-random currents in the somas. In particular, a detailed experimental analysis of the thalamic firing patterns under PD conditions [Magnin et al., 2000] classified neurons from the Vim in 4 groups based on the frequency and features of the spikes:

- **sporadic neurons:** they fire single spikes or duplets irregularly, i.e., their inter-spike interval (ISI) distribution is unimodal and the autocorrelation histogram flat;
- **random LTS bursting neurons:** they have autocorrelation histograms with only one peak and ISI histograms with a weak bimodal distribution. Bursting activity is due to low-threshold calcium currents;
- **rhythmic LTS bursting neurons:** as the previous group, but the autocorrelation histograms exhibit at least two successive peaks and the ISI histogram has a marked bimodal distribution;
- **tremor-locked bursting neurons:** they burst rhythmically locked with the forearm tremor at 4 Hz. Even if the firing pattern leads to ISI and autocorrelation histograms similar to those of the previous group, intrinsic features and ionic origins of the bursts are significantly different from the LTS case.

Intracellular currents were designed as random sequences of cathodic monopolar rectangular pulses. The pulse-width

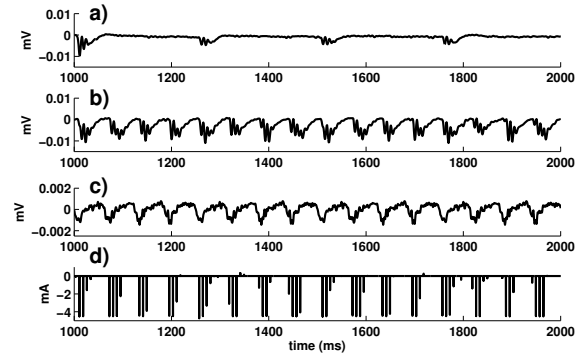


Fig. 4. Parkinsonian LFPs in R_1 when no DBS (a) or feedback control (b) was applied. The reference signal is in (c), I_{stim} in (d).

and the distribution of the inter-pulse intervals were chosen to reproduce the inter-burst features (i.e., firing rate, number of spikes per burst, shape of the ISI histogram) of original data in [Magnin et al., 2000]. For each population, the percentages of neurons assigned to each group were compliant with those reported in [Magnin et al., 2000] for the ventro-lateral posterior nucleus ventral division of the thalamus, roughly coincident with the Vim. The intra-burst features, instead, were neglected since of limited interest for the construction of the extracellular field potentials. Phase delays uniformly picked between 1 and 4 ms were applied to the intracellular currents to increase the variability across the neurons, while a white noise realization (mean $\mu = 0$ nA, variance $\sigma^2 = 3$) was injected into the somas to reproduce membrane voltage fluctuations (see [Kuncel et al., 2007] and references therein).

2.2 Minimum Prediction Error Identification

For each point R_i , $i = 1, 2, 3$ where the LFP was computed according to (1), the relationship between local field potential and extracellular stimulus was investigated. Input (extracellular stimulus) and output (LFP) signals were low-pass filtered (cutoff frequency: 100 Hz), downsampled to $f_s = 1250$ Hz and detrended. An ARX I-O model was then identified by minimizing the prediction error through the recursive least-squares (RLS) algorithm [Ljung, 1999]. The identification procedure used a 10000 ms-long quasi-white-noise-like input signal w to persistently excite the neural population. The time shape of w was designed as a sequence of 100 μ s-long monopolar cathodic rectangular pulses whose instantaneous frequency (i.e., the inverse of the ISI following the pulse) was uniformly chosen between the values: 10, 35, 60, 90, 130, and 185 Hz, which were experimentally proved to affect the tremor intensity in ET patients [Kuncel et al., 2007]. The pulse amplitudes, instead, were uniformly picked from the values required to activate 10%, 30%, 50%, 70%, and 90% of the neurons in each population with a train of 100 μ s-long cathodic rectangular pulses at 185 Hz. To improve the procedure, the I-O signals were split in 2 segments, one for identification (65% of the length) and the other for cross-validation (35%) purposes. The final model structure was:

$$A(z)y(k) = B(z)u(k-1) + \epsilon(k), \quad (2)$$

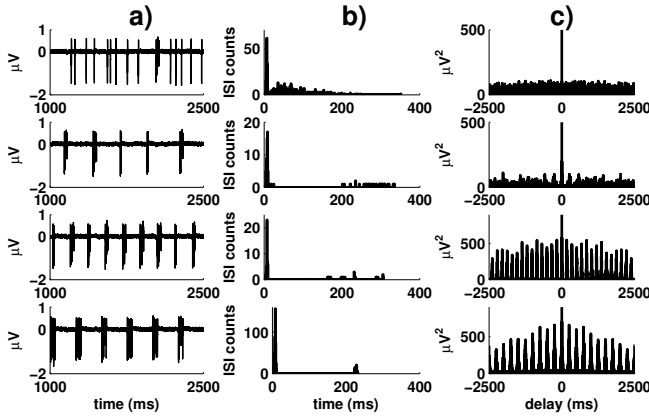


Fig. 5. (a) 4 types of firing neurons in the Vim. (b) ISI histograms (bin: 1 ms). (c) autocorrelation functions. From top to bottom: sporadic, random LTS bursting, rhythmic LTS bursting, and tremor-locked cells. Peak at 0 ms is truncated in the autocorrelation.

where $A(z) = 1 + a_1z^{-1} + \dots + a_{na}z^{-na}$ and $B(z) = b_0 + b_1z^{-1} + \dots + b_{nb-1}z^{-nb}$ are polynomials in the \mathcal{Z} -domain of order na and nb respectively, while $y(k)$ and $u(k)$ are the filtered output and input signal at time kT respectively, with T sampling time ($T = 1/1250 = 0.8$ ms). $\epsilon(k)$, instead, accounts for identification residuals, due to not modeled dynamics or exogenous inputs (e.g., synaptic input to the neural population). For control purposes it was assumed $na = 6$ and $nb = 1$ (see Section 2.3).

2.3 Control Scheme

Feedback control aimed at changing the overall electric behavior of the neural population and tracking the power spectrum of the reference signal. Moreover, it pursued robustness in goal achievement against model errors and measurement noise without affecting movement-related signals. For that reason, a model-based minimum variance control law was designed [Åström, and Wittenmark, 1995]. It reshaped the I-O relationship of the neural population and rearranged the power spectral density of the output. In details, the feedback loop in Fig. 3 was implemented, where the transfer functions $F(z)$, $G(z)$, and $H(z)$ were:

$$\begin{aligned} F(z) &= z \left(M_D(z) - \frac{A(z)M_N(z)}{\gamma_0} \right) \\ G(z) &= \frac{\gamma_0}{M_N(z)B(z)} \\ H(z) &= M_N(z) \end{aligned} \quad (3)$$

with $A(z)$, and $B(z)$ given by (2) and $M_N(z)$, and $M_D(z)$ being the numerator and denominator of the desired closed loop I-O transfer function respectively. To reduce the model order, it was fixed *a priori* $na = 6$ and $nb = 1$ in (2) because, independently of the position of the recording electrode and the neural population, such orders were proved to keep the prediction error power on the validation data lower than 1% of the true data power. Without loss of generality, it was assumed that:

$$\begin{aligned} M_N(z) &= \gamma_0 + \gamma_1z^{-1} + \dots + \gamma_{n_N}z^{-n_N} \\ M_D(z) &= 1 + \delta_1z^{-1} + \dots + \delta_{n_D}z^{-n_D} \end{aligned} \quad (4)$$

with n_N and n_D , γ_i $i = 0, \dots, n_N$ and δ_j $j = 1, \dots, n_D$ chosen so that the ratio $M_N(z)/M_D(z)$ was a 2nd order

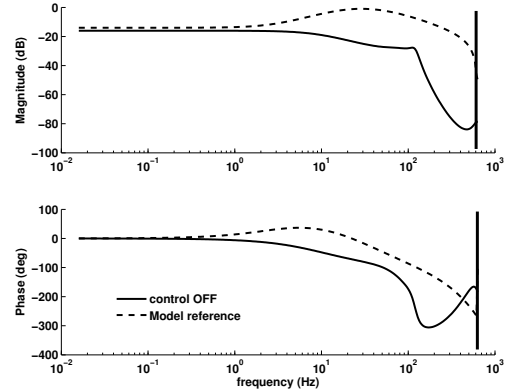


Fig. 6. Bode diagrams of the TF identified on data recorded by R_1 in disease conditions. “control OFF” curves refer to the TF identified by using signal w , while “Model reference” ones refer to $M_N(z)/M_D(z)$. The vertical bar marks the Nyquist frequency.

filter with cutoff frequencies $f_{inf} = 19$ Hz and $f_{sup} = 45$ Hz and gain 0.2. Such choice was due to the spectral properties of the reference signal (see Section 2.4 and 3) and the transfer function of the identified model.

In agreement with experiments in [Kuncel et al., 2006], the applied stimulus was modulated by multiplying the control signal by a train of pulses (Fig. 3). Pulse-width was 100 μ s, while the train’s frequency was set to an aliasing-free value (130 Hz). For safety purposes, the absolute value of the final input was limited to 4.5 mA. The control signal, instead, was prevented to become anodic due to the limits of the TC relay neuron model used in simulation, the properties of the input signal exploited in the identification experiments, and experimental data that proved anodic stimuli ineffective.

2.4 Reference Signal Generation

The reference signal for the control scheme was built in simulation starting from experimental data reported in [Molnar et al., 2005]. As done in Section 2.1 for PD tremor conditions, the intrinsic firing properties of the neurons were fit on single-unit data from literature and, then, simulated with no extracellular stimulating source applied. The LFPs correspondingly recorded by R_i , $i = 1, 2, 3$ according to (1), were low-pass filtered (cutoff frequency: 100 Hz), split into sections (250 ms-long each), and averaged over the sections. The resulting average signal was used as the template of the periodic reference signal in the fundamental period.

Data in [Molnar et al., 2005] come from TC relay neurons recorded in the Vim of patients not affected by movement-related diseases (chronic pain patients) and, to our knowledge, such data are weakly affected by the pain disorders. Neurons were divided into 2 groups: 74% of them were “kinesthetic” (i.e., the firing rate was responsive to passive joint movements imposed to the associated limb) and 26% “voluntary” (i.e., the firing rate was responsive to voluntary joint movements). For each group, then, neurons were further classified as “regular”, “random” or “irregular”. The definition of “regular”, “random” and “irregular” was

based on a simplified version of the burst analysis methods reported in [Kaneoke, and Vitek, 1996] and required the comparison of the spike density histograms experimentally built with Poisson distributions [Molnar et al., 2005].

In simulation, the percentage of neurons in each group was the same as in [Molnar et al., 2005], the groups were uniformly distributed in the volume, while the intracellular currents were defined as stochastic sequences of cathodic rectangular pulses whose duration and ISIs were chosen by fitting the average spiking/bursting rates and the spike density histograms on the experimental data in [Molnar et al., 2005]. $ref(k)$ was then obtained by low-pass filtering and downsampling the simulated signal as done before.

3. RESULTS

Neurons were uniformly distributed in the volume and the association between position and electric features of the cells was purely random. In this way, a homogeneous neural tissue around the electrodes was simulated, in agreement with single-unit analysis in [Magnin et al., 2000, Molnar et al., 2005]. The application of the burst analysis method by [Kaneoke, and Vitek, 1996] on the neurons producing the reference signal revealed that they had an average firing rate and ISI distribution similar to experimental data from [Molnar et al., 2005] (data not reported here). Independently of the position of the recording electrode and the specific population of neurons, the ultimate effect of this scenario was a LFP signal of low amplitude (see Fig. 4c) with a marked periodicity in the range [15, 20] Hz related to the average firing frequency of voluntary and kinesthetic neurons. In tremor conditions, instead, more complicated patterns were simulated. As reported in Fig. 5, sporadic neurons fired single spikes or duplets in a tonic way but the corresponding ISIs were not constant (flat histogram and autocorrelogram in the uppermost row of Fig. 5b, c). The other types, instead, had a marked bursting mode and were different one from another about the number of spikes per burst and the duration of the inter-burst interval (averaged values and variance as in [Magnin et al., 2000]). A comparison with results in [Magnin et al., 2000] showed that simulations are qualitatively consistent with experimental data.

3.1 Identification and Control

The I-O transfer function (TF) $B(z)/A(z)$ identified through the RLS algorithm with $na = 6$ and $nb = 1$ showed that in PD conditions the gain is low and flat on a large frequency range (see Fig. 6), thus accounting for the negative effects that DBS at frequencies less than 100 Hz usually has on motor disorders [Kuncel et al., 2006]. The peak of the magnitude diagram in the high frequency band ([100, 150] Hz), instead, denoted increased gain and might explain the responsiveness of the therapy for stimulation over 100 Hz. It is interesting to note that, even if the identification residuals obtained with an ARX(6, 1) did not pass whiteness and independence tests [Ljung, 1999], the prediction error was very small (its power was less than 1% of the total power of the cross-validation data set) while the power spectrum of the applied input was almost flat on the frequency range of useful biological signals (≤ 100 Hz). This means that the family of models ARX(6, 1), even if

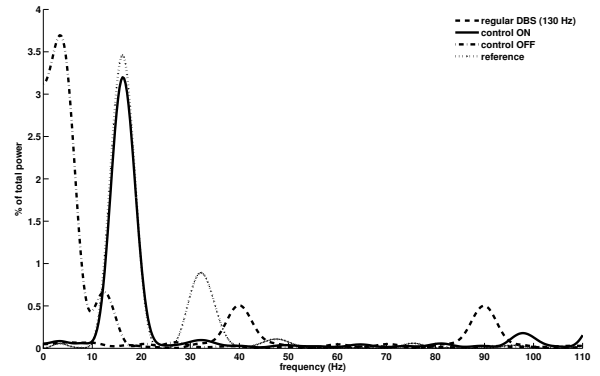


Fig. 7. Power spectrum of the reference signal (reference) and the LFPs recorded by electrode R_1 in disease conditions without (control OFF) or with adaptive (control ON) and actual (regular DBS) DBS input.

unable to exactly identify the I-O relationship on the Vim, gives a useful approximation for the frequencies of interest. In addition, it is worth to note that the purpose of our work was not the identification itself but the design of a model-based feedback control law: the simplified model structure, then, contributed to keep the controller order low. Possible mismatches or errors due to the model limits, however, were compensated by periodically updating the model parameters in the self-tuning scheme of Fig. 3 (update frequency: 1250 Hz). Independently of the used population, the control law modified the temporal profile of the LFPs in order to suppress tremor and restore disease-free conditions. Based on an average version of the field potentials in tremor-free settings, it paced the neural population and modulated the input amplitude to elicit bursts on a regular basis. Feedback information was used to synchronize the pattern of stimulation and update its value based on the detection of tremor-locked bursts (see Fig. 4, 7: the DBS was modulated (Fig. 4d) to elicit bursts at the same frequency as in disease-free settings (Fig. 4b, c) and restore the dominant components of the LFPs power spectrum by cleaning up the content in the tremor band ([2, 7] Hz) but not in the α and β bands, where voluntary movement signals to the Vim usually have significant spectral content (the second peak in Fig. 7 is of secondary concern for the motor commands). A comparison with the results obtained when the actual DBS was applied (i.e., regular train of cathodic pulses of 4.5 mA at 130 Hz) indicates that feedback control contributes to better recover tremor-free conditions instead of introducing an information lesion from 8 to 30 Hz (see Fig. 7).

4. CONCLUSIONS

Our study proved that the local field potentials recorded in the Vim can be used as a feedback variable for the automatic calibration of the DBS to suppress tremor in PD conditions. In particular, it showed that a black box identification approach can describe the relationship between extracellular stimulating current and LFPs through an ARX model and that, based on it, a minimum variance feedback control law can be designed to update the stimulus and restore reference spectral properties. The identified

model was focused on that dominant dynamics in the Vim electric activity which can be evaluated from the LFPs, i.e., the proposed model neglected the cellular effects of the DBS and the topological organization of the stimulated nuclei, while described the overall changes induced by the stimulation. For that reason, even if simulations were performed with no synapsis added or network effects, minor discrepancies in the LFPs behavior are expected.

The reference signal, instead, was averaged from single-unit data and described the main rhythms that are usually common in all the subjects not affected by movement disorders. The latter aspect and the use of a point-wise approximation for the electrodes may represent a limit for our simulations and requires further analysis through a more detailed description of the geometry and orientation of the electrodes via finite elements analysis. After that, an experimental validation will be mandatory to test the actual effects of the control scheme on tremor and other movement disorders.

ACKNOWLEDGEMENTS

Authors gratefully acknowledge Prof. W.M. Grill for helpful support, suggestions, and comments on the manuscript.

REFERENCES

- V.C. Anderson, K.J. Burchiel, P. Hogarth, J. Favre, and J.P. Hammerstad. Pallidal vs subthalamic nucleus deep brain stimulation in Parkinson's disease. *Arch Neurol*, 62:554–560, 2005.
- K.J. Åström, and B. Wittenmark. *Adaptive Control*, 2nd Edition. Addison-Wesley, Boston, MA (USA), 1995.
- C. Beurrier, P. Congar, B. Bioulac, and C. Hammond. Subthalamic nucleus neurons switch from single-spike activity to burst-firing mode. *J Neurosci*, 19:599–609, 1999.
- S. Bittanti, and M. Campi. Least-squares based self-tuning control systems. In S. Bittanti and G. Picci, editor, *Identification, Adaptation, Learning*, NATO ASI Series F, volume 153, pages 339–365. Springer, New York, NY (USA), 1994.
- N.T. Carnevale, and M.L. Hines. *The Neuron Book*. Cambridge University Press, Cambridge, UK, 2006.
- A. Destexhe, M. Neubig, D. Ulrich, and J. Huguenard. Dendritic low-threshold calcium currents in thalamic relay cells. *J Neurosci*, 18:3574–3588, 1998.
- J.O. Dostrovsky, and A.M. Lozano. Mechanisms of deep brain stimulation. *Mov Disord*, 17 (Suppl 3):63–68, 2002.
- C. Halpern, H. Hurtig, J. Juggi, M. Grossman, M. Won, and G. Baltuch. Deep brain stimulation in neurologic disorders. *Parkinsonism Relat Disord*, 13:1–16, 2007.
- T. Hashimoto, C.M. Elder, M.S. Okun, S.K. Patrick, and J.L. Vitek. Stimulation of the subthalamic nucleus changes the firing pattern of pallidal neurons. *J Neurosci*, 23:1916–1923, 2003.
- S.E. Hua, and F.A. Lenz. Posture-related oscillations in human cerebellar thalamus in essential tremor are enabled by voluntary motor circuits. *J Neurophysiol*, 93:117–127, 2005.
- E.R. Kandel, J.H. Schwartz, and T.M. Jessell. *Principles of Neural Science*, Fourth Edition. McGraw-Hill Health Professions Division, New York, NY (USA), 2000.
- Y. Kaneoke, and J.L. Vitek. Burst and oscillation as disparate neuronal properties. *J Neurosci Methods*, 68: 211–223, 1996.
- R. Kumar, A.M. Lozano, E. Sime, and A.E. Lang. Long-term follow-up of thalamic deep brain stimulation for essential and parkinsonian tremor. *Neurology*, 61:1601–1604, 2003.
- A.M. Kuncel, S.E. Cooper, B.R. Wolgamuth, M.A. Clyde, S.A. Snyder, E.B. Montgomery, A.R. Rezai, and W.M. Grill. Clinical response to varying the stimulus parameters in deep brain stimulation for essential tremor. *Mov Disord*, 21:1920–1928, 2006.
- A.M. Kuncel, S.E. Cooper, B.R. Wolgamuth, and W.M. Grill. Amplitude- and frequency-dependent changes in neuronal regularity parallel tremor with thalamic deep brain stimulation. *IEEE Trans Neural Syst Rehabil Eng*, 15:190–197, 2007.
- F.A. Lenz, R.R. Tasker, H.C. Kwan, S. Schneider, R. Kwong, Y. Murayama, J.O. Dostrovsky, and J.T. Murphy. Single unit analysis of the human ventral thalamic nuclear group: correlation of thalamic “tremor cells” with the 3-6 Hz component of parkinsonian tremor. *J Neurosci*, 8:754–764, 1988.
- L. Ljung. *System Identification: Theory for the User*. Prentice Hall PTR, Upper Saddle River, NJ (USA), 1999.
- M. Magnin, A. Morel, and D. Jeanmonod. Single-unit analysis of the pallidum, thalamus and subthalamic nucleus in parkinsonian patients. *Neuroscience*, 96:549–564, 2000.
- C.C. McIntyre, W.M. Grill, D.L. Sherman, and N.V. Thakor. Cellular effects of deep brain stimulation: model-based analysis of activation and inhibition. *J Neurophysiol*, 91:1457–1469, 2004.
- S. Miocinovic, M. Parent, C.R. Butson, P.J. Hahn, G.S. Russo, J.L. Vitek, and C.C. McIntyre. Computational analysis of subthalamic nucleus and lenticular fasciculus activation during therapeutic deep brain stimulation. *J Neurophysiol*, 96:1569–1580, 2006.
- G.F. Molnar, A. Pilliar, A.M. Lozano, and J.O. Dostrovsky. Differences in neuronal firing rates in pallidal and cerebellar receiving areas of thalamus in patients with Parkinson's disease, essential tremor, and pain. *J Neurophysiol*, 93:3094–3101, 2005.
- E. Moro, R.J.A. Esselink, J. Xie, M. Hommel, A.L. Benabid, and P. Pollak. The impact on Parkinson's disease of electrical parameter settings in STN stimulation. *Neurology*, 59:706–713, 2002.
- A. Nambu, and R. Llinás. Electrophysiology of globus pallidus neurons in vitro. *J Neurophysiol*, 72:1127–1139, 1994.
- A. Priori, G. Ardolino, S. Marceglia, S. Mrakic-Sposta, M. Locatelli, F. Tamma, L. Rossi, and G. Foffani. Low-frequency subthalamic oscillations increase after deep brain stimulation in Parkinson's disease. *Brain Res Bull*, 71:149–154, 2006.
- S. Sato, M. Parent, M. Lévesque, and A. Parent. Axonal branching pattern of the subthalamic nucleus in primates. *J Comp Neurol*, 424:142–152, 2000.
- T. Wichmann, and M.R. DeLong. Deep brain stimulation for neurologic and neuropsychiatric disorders. *Neuron*, 52:197–204, 2006.